CrossMark
click for updates

Cryptococcus neoformans Host Adaptation: Toward Biological Evidence of Dormancy

Alexandre Alanio,[a,b,c,d] Frédérique Vernel-Pauillac,[a,b] Aude Sturny-Leclère,[a,b] Françoise Dromer[a,b]

Institut Pasteur, Molecular Mycology Unit[a]; CNRS URA3012[b]; Laboratoire de Parasitologie-Mycologie, Hôpital Saint-Louis, Groupe Hospitalier Lariboisière, Saint-Louis, Fernand Widal, Assistance Publique-Hôpitaux de Paris (AP-HP)[c]; Université Paris Diderot, Sorbonne Paris Cité, Paris, France[d]

ABSTRACT Cryptococcosis is an opportunistic infection due to the ubiquitous yeast *Cryptococcus neoformans*. This yeast inter-acts closely with innate immune cells, leading to various fates, including fungal persistence within cells, making possible the dis-semination of the yeast cells with monocytes via a Trojan horse strategy. In humans, the natural history of the infection begins with primoinfection during childhood, which is followed by dormancy and, in some individuals, reactivation upon immunosup-pression. To address the question of dormancy, we studied *C. neoformans* infection at the macrophage level (*in vitro* H99-macrophage interaction) and at the organ level in a murine model of cryptococcosis. We analyzed the diversity of yeast adapta-tion to the host by characterizing several *C. neoformans* populations with new assays based on flow cytometry (quantitative flow cytometry, multispectral imaging flow cytometry, sorting), microscopy (dynamic imaging), and gene expression analysis. On the basis of parameters of multiplication and stress response, various populations of yeast cells were observed over time *in vivo* and *in vitro*. Cell sorting allowed the identification of a subpopulation that was less prone to grow under standard conditions than the other populations, with growth enhanced by the addition of serum. Gene expression analysis revealed that this population had specific metabolic characteristics that could reflect dormancy. Our data suggest that dormant yeast cells could exist *in vitro* and *in vivo*. *C. neoformans* exhibits a huge plasticity and adaptation to hosts that deserves further study. *In vitro* generation of dormant cells is now the main challenge to overcome the limited number of yeast cells recovered in our models.

IMPORTANCE *Cryptococcus neoformans* is a sugar-coated unicellular fungus that interacts closely with various cells and organ-isms, including amoebas, nematodes, and immune cells of mammals. This yeast is able to proliferate and survive in the intracel-lular environment. *C. neoformans* causes cryptococcosis, and yeast dormancy in humans has been suggested on the basis of epi-demiological evidence obtained years ago. By studying an *in vitro* model of yeast-macrophage interaction and murine models of cryptococcosis, we observed that yeast cells evolve in heterogeneous populations during infection on the basis of global meta-bolic activity. We compared the growth ability and gene expression of yeast cells belonging to various populations in those two models. We eventually found a population of yeast cells with low metabolism that fit some of the criteria for dormant cells. This paves the way for further characterization of dormancy in *C. neoformans*.

Cryptococcus neoformans is a basidiomycetous opportunistic yeast present in the environment. This fungus can survive predation by various organisms, ranging from protozoans to metazoans, through ready-made virulence traits (1). *C. neofor-mans* interacts closely with unicellular organisms (amoebas, par-amecia) (2–4) and with cells dedicated to the innate immune re-sponse (macrophages or dendritic cells) exhibiting various propensities of phagocytosis and intracellular killing (5, 6). Intra-cellular persistence in immune cells provides advantages to the fungus by allowing escape of the immune response and subse-quent dissemination (7, 8). In humans, contamination usually begins with the inhalation of basidiospores or desiccated yeast cells (9). Primoinfection occurs in childhood with unrecognized pneumonia (10). Yeast cells are then controlled by the immune system through granuloma formation (11) and adaptive immu-

nity with production of antibodies against *C. neoformans* proteins (10). From then on, until immunosuppression occurs, the yeast cells remain invisible and dormant, as demonstrated epidemio-logically (12, 13), and the infection is latent (14). When or if im-munodeficiency occurs, yeast cells reactivate and replicate proba-bly in the lung and disseminate through the bloodstream to different organs. Crossing of the blood-brain barrier leads to me-ningoencephalitis, the most common and severe clinical presen-tation (9, 15–17).

The pathophysiology of the infection has been studied experi-mentally in rats that naturally control *C. neoformans* lung infec-tion and more extensively in mice that are highly susceptible to infection. The fate of the infection depends on both host and mi-crobial factors. Virulence factors influence the outcome of infec-tion in the murine model of cryptococcosis (18) but also *in vitro*

and in humans (19). Microbial adaptation to the host is complex and has been studied as a whole in the lungs by histopathology (20) and by transcriptome analysis upon early infection (21). More recently, a particular adaptation to hosts was uncovered with the formation of titan cells in the lungs of infected mice (22, 23). These extraordinary enlarged yeast cells have specific properties that promote disease by preventing phagocytosis and clearance from the lung (24). However, we still do not know whether they really play a role in the persistence of the infection *in vivo*. Although extensive studies of *C. neoformans*-macrophage interactions and cryptococcosis have been performed with mice, no tangible biological evidence of dormancy has been brought to light. Our hypothesis is that populations of yeast cells with various metabolic states coexist in tissues after infection, with some yeast cells being dormant. We took advantage of assays and models previously implemented in the laboratory (19, 25, 26) to test this hypothesis and developed tools to analyze yeast cells at the single-cell level or after sorting of a low number of specific cell populations. In the lungs of infected mice and upon macrophage interaction, we uncovered a subpopulation of yeast cells exhibiting low metabolic activity and delayed growth rescued by the addition of serum that fit the criteria of a dormant phenotype.

RESULTS

Implementation of a new flow cytometry assay to analyze multiplication and stress responses simultaneously in *C. neoformans*. To study *C. neoformans* adaptation to different environments, we first developed an assay that combined multiplication and stress response analyses.

Multiplication was quantified on the basis of the decrease in calcofluor (CALCO) fluorescence intensity over time with the appearance of a population with a lower CALCO fluorescence intensity (CALCO$^{med+low}$; daughter cells) and the persistence of the highly stained population (CALCO^{high}; mother cells) (19). The proportion of daughter cells increased over time in standard yeast extract-peptone-dextrose (YPD) cultures, inside J774 cells, and in the lungs of infected mice (Fig. 1A).

The stress response was evaluated with 5-chloromethylfluorescein diacetate (CMFDA), which measured a glutathione-dependent phenomenon, as shown by a preliminary experiment with diethyl maleate, a glutathione-depleting agent (see Fig. S1A in the supplemental material). *C. neoformans* cells in stationary phase (baseline, H0) harbored basal fluorescence that increased over time with various stresses (water, hydrogen peroxide, fresh medium, and heat) (Fig. 1B). Of note, after 24 h of incubation in hydrogen peroxide, the CMFDA fluorescence level was comparable to that of unstained condition (Fig. 1B, dark green histogram, right upper panel), with culture revealing that all of the yeast cells were dead (data not shown). The level of CMFDA fluorescence depended on the stimulus, with yeast nitrogen base (YNB) medium inducing the lowest and hydrogen peroxide the highest stress response (Fig. 1B; see Fig. S1B).

The viability of yeast cells was assessed on the basis of Topro-3 iodide (TOPRO) fluorescence intensity (Fig. 1C), allowing exclusion of dead cells in all subsequent experiments.

Dynamics of *C. neoformans* host adaptation. We studied yeast cell adaptation to host in terms of yeast multiplication and stress responses, looking for changes over time *in vitro* (J774 macrophages) and *in vivo* (lungs of mice) (Fig. 2).

A population of daughter yeast cells was observed as soon as 2 h after interaction with J774 cells and 15 h in lungs (Fig. 2A and C) and increased over time (Fig. 2B and D). An increase in CMFDA fluorescence intensity was observed in *C. neoformans* cells after 2 h of interaction with J774 cells and after 7 h in the lungs of infected mice, with the majority of the population remaining CMFDA^{high} over time. However, a subpopulation with a lower CMFDA fluorescence level (CMFDA$^{med+low}$, black arrows) appeared at 24 h in J774 cells and at 30 h in lungs and increased over time. This phenomenon affected first mother cells (24 h) and then daughter cells (48 h) in J774 cells and both populations at 30 h in lungs.

Subsequent experiments were done with mice inoculated 7 days before, on the basis of the assumption that dormant cells should already be present and in sufficient number for further analysis. *C. neoformans* multiplication and stress responses were then assessed in the brains, lungs and spleens of 6 OF1 mice (Fig. 3) and analyzed individually by classical flow cytometry (Macsquant analyser; Miltenyi Biotec). Mother cells were not observed in the brains, were rare in the spleens, and were present in the lungs of 4/6 OF1 mice (Fig. 3, gated population). The stress response pattern differed among the lungs, spleens, and brains but looked specific for each organ with several circumscribed populations in the lungs of 5/6 mice. Of note, under the same conditions, no mother cell population was detected in the organs of BALB/c mice; this is potentially related to their more acute infection (data not shown).

We thus decided to explore morphological and biological features of the viable yeast cells present in the lungs of infected mice by multispectral imaging flow cytometry (Imagestream^X) and pooled lung homogenates (Fig. 4 and 5; see Fig. S2 to S5 in the supplemental material). After determination of the analysis strategy (see Fig. S2), including an optical control, we defined nine populations of yeast cells (CALCO high, medium, and low) with various (high, medium, and low) levels of CMFDA fluorescence intensity on the CMFDA/CALCO dot plot (Fig. 4A and B; see Fig. S3A and B). Daughter cells always represented less than 20% of the three CMFDA populations. Mother cells represented more than half of the CMFDA^{high} population and less than 40% of the others (Fig. 4B). The global analysis of morphological features (54 algorithms) revealed five clusters composed mainly of daughter cells, mother cells, CMFDA^{high}, CMFDA^{med}, and CMFDA^{low} populations (Fig. 4C). The largest yeast cells were composed mostly of mother cells (Fig. 4C, cluster h, red outline), but a subpopulation of mother cells was small yeast cells (see Fig. S3C and D). Daughter cells were composed mostly of small yeast cells (Fig. 4C, cluster h, pink outline) and yeast cells with a specific morphology (Fig. 4C, cluster b, red outline). Apart from mother and daughter cells, CMFDA^{low} populations harbored specific morphological features (Fig. 4C, cluster c, red outline).

Analysis of specific *C. neoformans* populations. To go further into the analysis of the different populations, we focused first on the CMFDA^{high}/mother cell population (Fig. 5). Two patterns of CMFDA fluorescence were visualized by Imagestream^X (Fig. 5A) and microscopy (Fig. 5B), with some cells with peripheral extracellular fluorescence (designated "surrounded") and others intracellular fluorescence ("intracellular"). These two populations were delineated on the basis of the modulation (texture) and the area (size) dot plot algorithms (Fig. 5C).

The majority of mother cells were found to have intracellular CMFDA. Yeast cells with a surrounded CMFDA were composed of similar proportions of mother and daughter cells (see Fig. S4 in the supplemental material), and some yeast cells exhibited a pe-
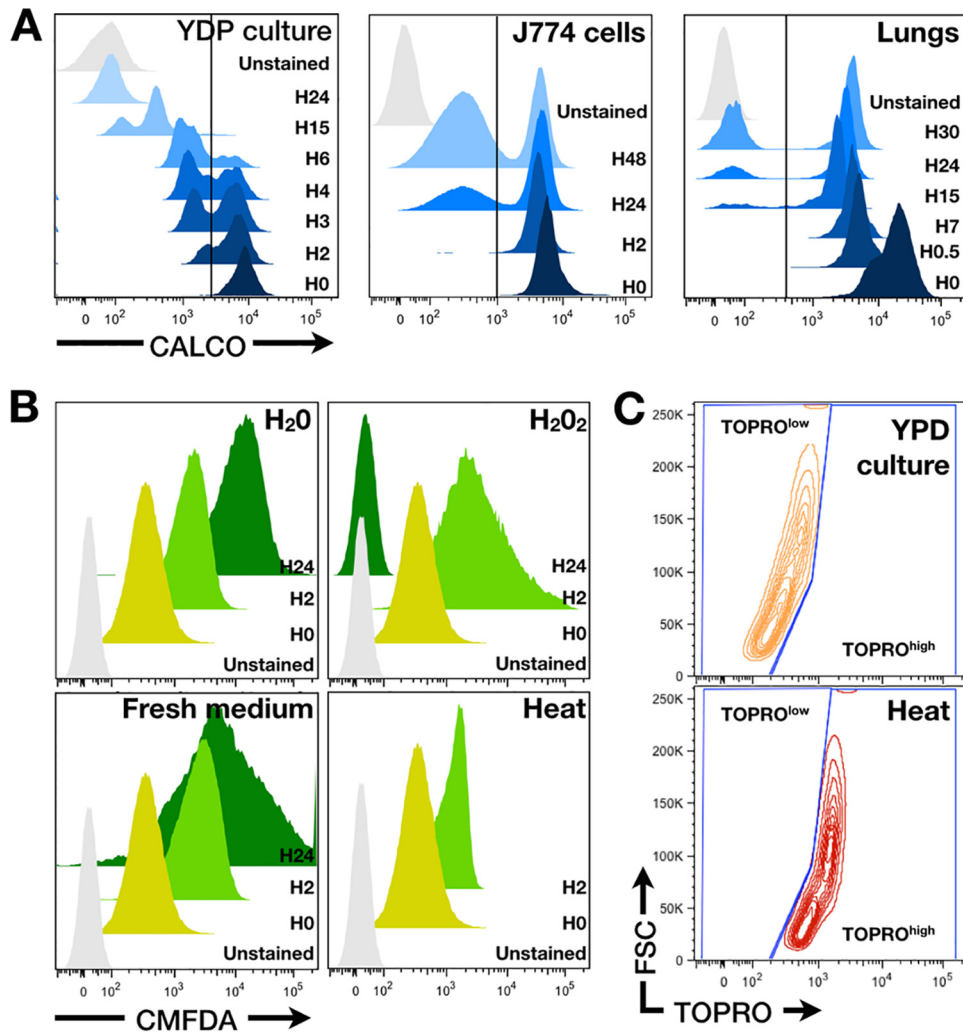
FIG 1 Quantification of *C. neoformans* (H99) multiplication, stress response, and viability with fluorescent dyes and flow cytometry. (A) *C. neoformans* multiplication was evaluated after Calcofluor (CALCO) staining of yeast cells prior to incubation into YPD medium, interaction with murine macrophages, or inoculation to outbred OF1 mice. The yeast cells were recovered from different environments (YPD culture, J774 cells, and lungs) at different time points and compared to unstained yeast cells by flow cytometry (MacsQuant analyzer, Miltenyi Biotec). A population with lower CALCO fluorescence intensity (daughter cells) appeared over time under the three conditions. Gates allowing segregation of CALCO^{high} and CALCO$^{med+low}$ cells are depicted for each condition (YPD culture, J774 cells, and lungs). Of note, the decrease in CALCO fluorescence intensity observed in yeast cells recovered from lungs as soon as 30 min after inoculation can be attributed to quenching and not to multiplication. (B) *In vitro C. neoformans* stress response evaluated on the basis of CMFDA staining. Yeast cells were stained with CMFDA (10 μM) for 30 min at 37°C. Various stresses (H$_2$O, H$_2$O$_2$, fresh medium [DMEM–10% FCS–1% penicillin/streptomycin] and heat killing [HK]) were applied to stationary-phase (H0) yeast cells for 2 and 24 h (H24). CMFDA fluorescence increased over time, except at H24 after H$_2$O$_2$ incubation, where it became negative. (C) Viability of *C. neoformans* populations was assessed with Topro-3 iodide (TOPRO) with dead yeast cells (HEAT) with a higher fluorescence intensity (TOPRO^{high}) than viable yeast cells harvested in stationary phase upon standard culture (YPD culture, TOPRO^{low}).

culiar morphology by Imagestream^X (Fig. 5B) and interference contrast microscopy (Fig. 6A). These cells (Drop Cn in Fig. 6) were small (5.80 $\pm$ 0.80 μm) with an enlarged cell wall and a well-defined round refringent vesicle. This population was composed of a higher proportion of mother cells than *C. neoformans* cells with a regular morphology (Reg Cn in Fig. 6) (see Fig. S4B). Drop *C. neoformans* cells represented less than 25% of each CMFDA population (Fig. S4C). Compared to regular *C. neoformans* cells, drop *C. neoformans* did not harbor a well-organized nucleus (4′,6-diamidino-2-phenylindole [DAPI] staining), had a low RNA content (SYTO 85) and mitochondrial activity (Mitotracker) and exhibited a complete retraction of the cytoplasm around the central vesicle (MDY64, Fig. 6B and C). These obser-

vations suggested that drop *C. neoformans* were dead yeast cells with low transcriptional and mitochondrial activity, and disorganized cytoplasm and nucleus architectures, despite having been initially selected in the TOPRO^{low} (viable) population. This was confirmed by dynamic imaging after observation that drop *C. neoformans* cells from lung homogenates were unable to bud over 48 h (data not shown).

Additional experiments showed that the relative proportion of the different yeast cell populations in terms of multiplication and stress response (see Fig. S5A to D), and the proportion of drop *C. neoformans* (see Fig. S5A) varied among *C. neoformans* strains, when comparing H99 and two previously characterized clinical isolates (19).
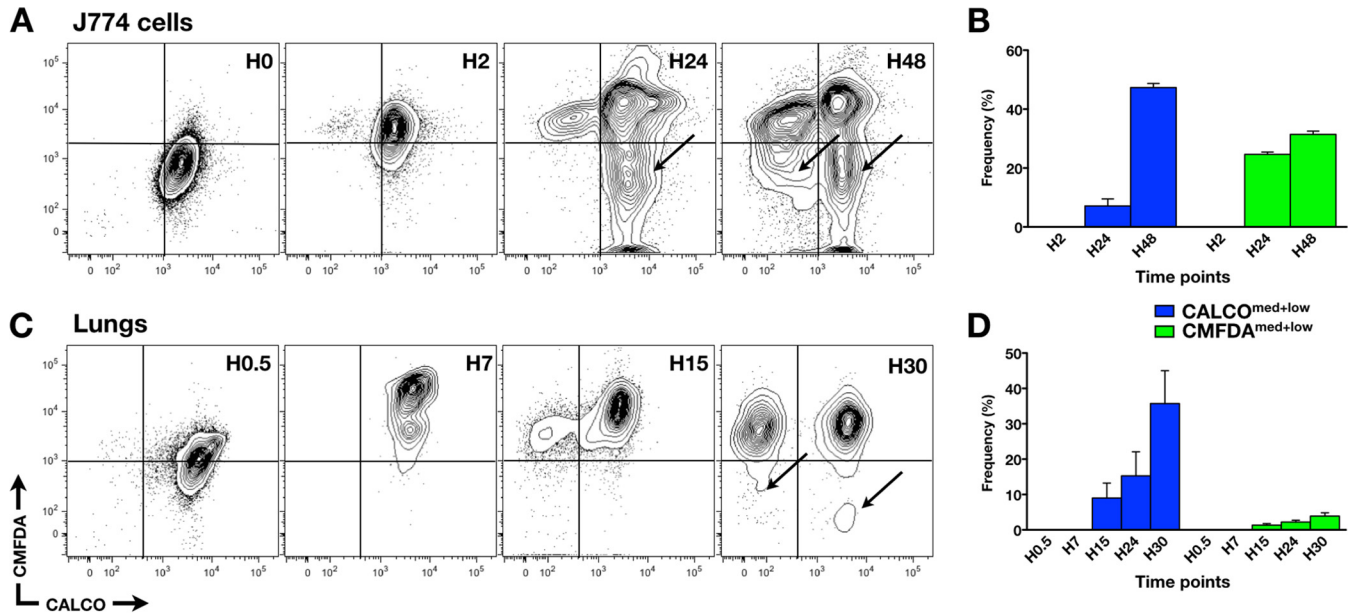
FIG 2 Evolution of *C. neoformans* multiplication and stress response in two host environments. The CALCO and the CMFDA fluorescence intensities were analyzed after interaction with macrophages (A and B) and in lungs of infected mice (C and D). After macrophage lysis or organ grinding, the pellet of yeast cells was stained with CMFDA (10 μM) and TOPRO (10 μM) for 30 min at 37°C (CMFDA/TOPRO assay). Analysis of the fluorescence was performed by flow cytometry after exclusion of the TOPRO^{high} population (dead yeast cells). The generation of daughter cells (CALCO$^{med+low}$) was noticed upon 2 h of macrophage interaction (A) and 15 h after mouse inoculation (C) and increased over time (B and D). An increased stress response (higher CMFDA fluorescence) was already seen at 2 h (H2) in macrophages (A) and 7 h (H7) in the lungs (B). A population with a lower CMFDA fluorescence level (CMFDA$^{med+low}$) (arrows) was observed at 24 h (H24) in macrophages (A and B) and at 30 h (H30) in lung cells (C and D) that affected first mother cells (24 h [H24]) and then daughter cells (48 h [H48]) in macrophages.

Specific phenotype of the CMFDA^{low} population. Cell sorting was implemented to focus on and compare the CMFDA^{low} population to the other populations recovered from both models of host interaction (24-h incubation with macrophages or lungs recovered on day 7 after inoculation of OF1 mice) and to monitor yeast cells in stationary phase all stained under the same conditions (Fig. 7) and monitored visually by fluorescence microscopy (see Fig. S6 in the supplemental material). We wondered whether the sorted populations harbored specific phenotypes in terms of growth capacity and transcriptional activity.

Growth curves analysis revealed important differences among the various populations. Indeed, the CMFDA^{low} population was unable to grow when recovered from mice (mice_CMFDA^{low}) or exhibited delayed growth when recovered from macrophages (macrophage_CMFDA^{low}) in YPD compared to that of other populations and control yeast cells (Fig. 7). Addition of fetal calf serum (FCS) restored growth for the population of mice_C-MFDA^{low} and markedly accelerated growth of all of the populations, including that of control yeast cells. Of note, the growth of the CMFDA^{med} and CMFDA^{high} populations was delayed in mice, but not in macrophages, compared to that of control yeast cells (Fig. 7B and D), while both populations behaved similarly under each condition (macrophages or mice).

The expression of 37 selected genes in the above-described populations was performed by real-time quantitative PCR (Fig. 8). Hierarchical clustering of yeast cell populations revealed that the CMFDA^{med} and CMFDA^{high} populations were closely related under both the macrophage and mouse conditions. Overall, four groups/populations were delineated: mice_CMFDA$^{high/med}$, macrophage_CMFDA$^{high/med}$, mice_CMFDA^{low}, and mac-

rophage_CMFDA^{low}. Of note, the CMFDA^{high} population clustered with control yeast cells (data not shown). Hierarchical clustering of genes revealed four clusters, with two clusters of particular interest, cluster 1 (C1) and C4 (Fig. 8; see Fig. S7 in the supplemental material). C1 was composed of genes known to be upregulated in the lungs during early infection (21). C4 included genes that were expressed more in the macrophage_CMFDA^{low} population. Finally, *PCK1* downregulation and *COX1* upregulation were observed only in the mice_ and macrophage_ CMFDA^{low} population.

DISCUSSION

Rapid overview of the published literature on *C. neoformans* and cryptococcosis clearly shows the complexity and the diversity of the host-yeast interplay. On the host side, a number of organisms are potentially exposed to *C. neoformans* (27, 28), variable susceptibility to infection (29, 30) and clinical presentation (31) are reported in humans, and differences in the interaction between yeast and immune cells are well established (5, 32, 33). On the fungal side, the diversity is also noticeable on several levels: genome (34), genotypes (35), capsule structure (36, 37), production of other virulence factors (38, 39), interaction with hosts cells (19, 40, 41), virulence in mice (19, 41), and microevolution during infection (5, 42, 43). Fungal adaptation to specific host environments has also been demonstrated (21, 25, 44, 45) without a focus on specific subpopulations of yeast cells, except for the titan cells that have been initially reported in the lungs of infected mice (22, 23).

There is no consensus on the definition of dormancy/quiescence. Most often, dormant cells are characterized by a low met-
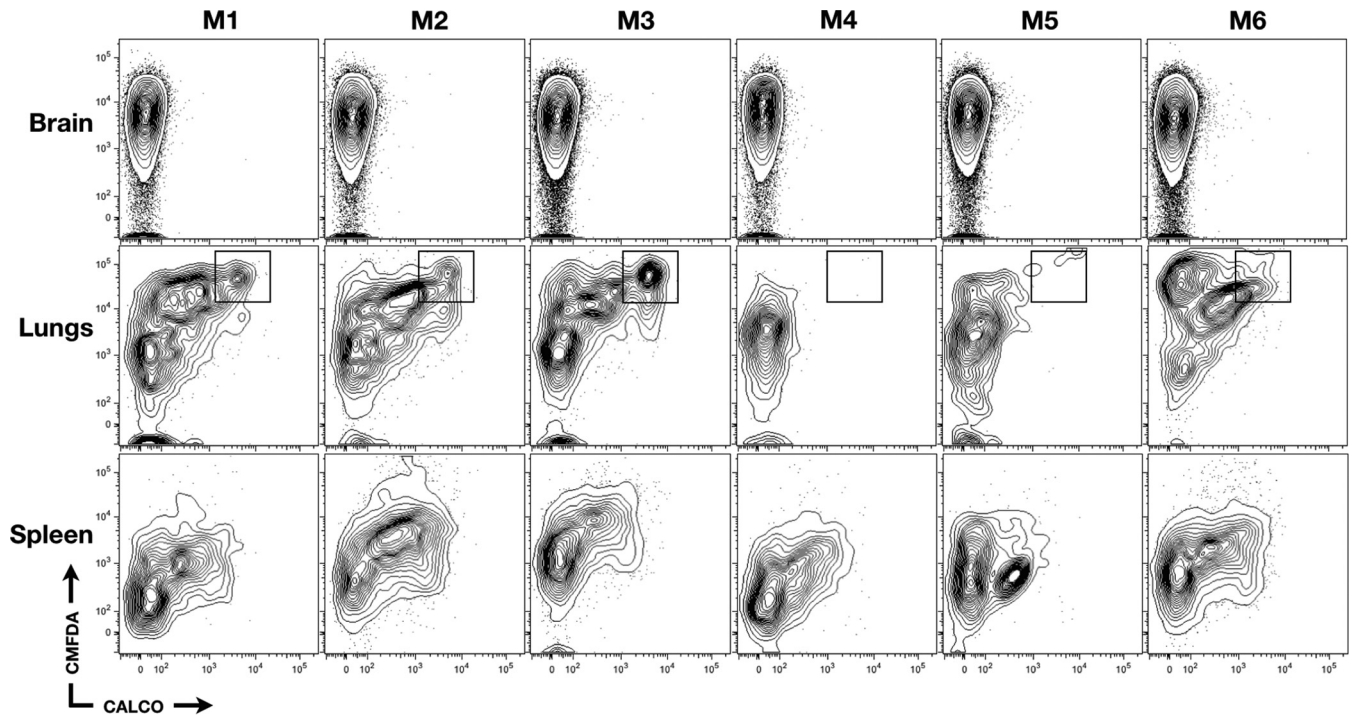
FIG 3 *C. neoformans* stress response and multiplication depends on individuals (outbred OF1 mice) and tissues. Seven days after inoculation with 10^5 CALCO-stained yeast cells (H99), mice were sacrificed and their organs (brains, lungs, and spleens) were ground. Yeast cells were stained for stress response and viability by CMFDA/TOPRO assay. Flow cytometry analysis was performed after exclusion of the TOPRO^{high} population (dead yeast cells) (MacsQuant analyzer; Miltenyi Biotec). The *C. neoformans* brain and spleen profile was homogeneous in terms of multiplication and stress response, whereas two profiles were observed in lungs. A well-defined CALCO^{high}/CMFDA^{high} population (black gate) was observed in some mice (M1 and M2, M3, and M5) and not in others (M4 and M6).

abolic activity sometimes undetectable under normal laboratory conditions (46) and the ability to be resuscitated by adequate stimuli (47). Dormancy has already been described in a wide range of organisms, including bacteria (46) (*Bacillus* spp., *Clostridium difficile*, *Chlamydia* spp., *Vibrio* spp., *Pseudomonas* spp.), mycobacteria (*Mycobacterium tuberculosis* [47–49]), apicomplexan parasites (in particular, *Plasmodium* spp. [50]), and fungi (*Saccharomyces cerevisiae* [51], *Schizosaccharomyces pombe* [52], *Aspergillus fumigatus* [53], or *Neurospora crassa* [54] spores). In *C. neoformans*, dormancy has only been demonstrated epidemiologically (12) and evoked for basidiospores (55).

We hypothesized that metabolically different subpopulations of yeast cells coexist in organs upon infection with the ambition to identify a population of yeast cells with low metabolic activity through a combination of selected reagents and techniques (dyes respecting yeast viability, multispectral imaging flow cytometry, dynamic imaging, single-cell real-time quantitative PCR protocols, cell sorting, growth curves).

The approach used was first to quantify yeast cell multiplication and stress response on the basis of CALCO and CMFDA staining, respectively. CALCO staining was used to track mother cells (CALCO^{high}, i.e., those that were inoculated), allowing us to compare stress responses in mother and daughter cells (19). CMFDA has previously been used in mammalian and fungal cells to quantify glutathione (56–58) or as a long-term cell tracker since it preserves viability (59). Glutathione is a nonenzymatic defense against oxidative stress. We showed here that *C. neoformans* responded to various stresses by increasing glutathione content. Exposure to protracted or violent stress (hydrogen peroxide) emp-

tied the pool of glutathione in *C. neoformans*, as it does in *S. cerevisiae* (60, 61).

An intriguing observation was the surrounded and not cytoplasmic pattern of CMFDA fluorescence associated with yeast cells with a specific morphology (drop *C. neoformans*) in the lungs. The peripheral extracellular staining could be related to either excretion of glutathione or diffusion of the host's glutathione during infection or sample processing. However, the use of various dyes evaluating metabolic activity and cell architecture, as well as dynamic imaging, strongly suggested that drop *C. neoformans* cells were mostly dead mother cells. This conclusion does not contradict the negative TOPRO staining, since negative DAPI and SYTO 85 staining suggested complete loss of nucleic acids in the drop *C. neoformans*. It is noteworthy that yeast cells looking like drop *C. neoformans* cells are brought out as typical cells of *C. neoformans* in many publications.

In addition to differences in morphology, analysis of multiplication and stress responses revealed the coexistence of several subpopulations of yeast cells that evolved over time in the host. The proportions of the various cell populations also varied with the host (OF1 versus BALB/c), tissue (lung versus brain), model (*in vitro* versus *in vivo*), and *C. neoformans* strain (H99 versus well-characterized clinical isolates). This clearly underscores the fact that findings on global *C. neoformans* adaptation to various environments should be interpreted with caution.

Sorting of the various populations of yeast cells may thus help in understanding *C. neoformans* biology in the host. The commonly accepted pathophysiology is that most cases of cryptococcosis result from the reactivation of dormant yeast cells without
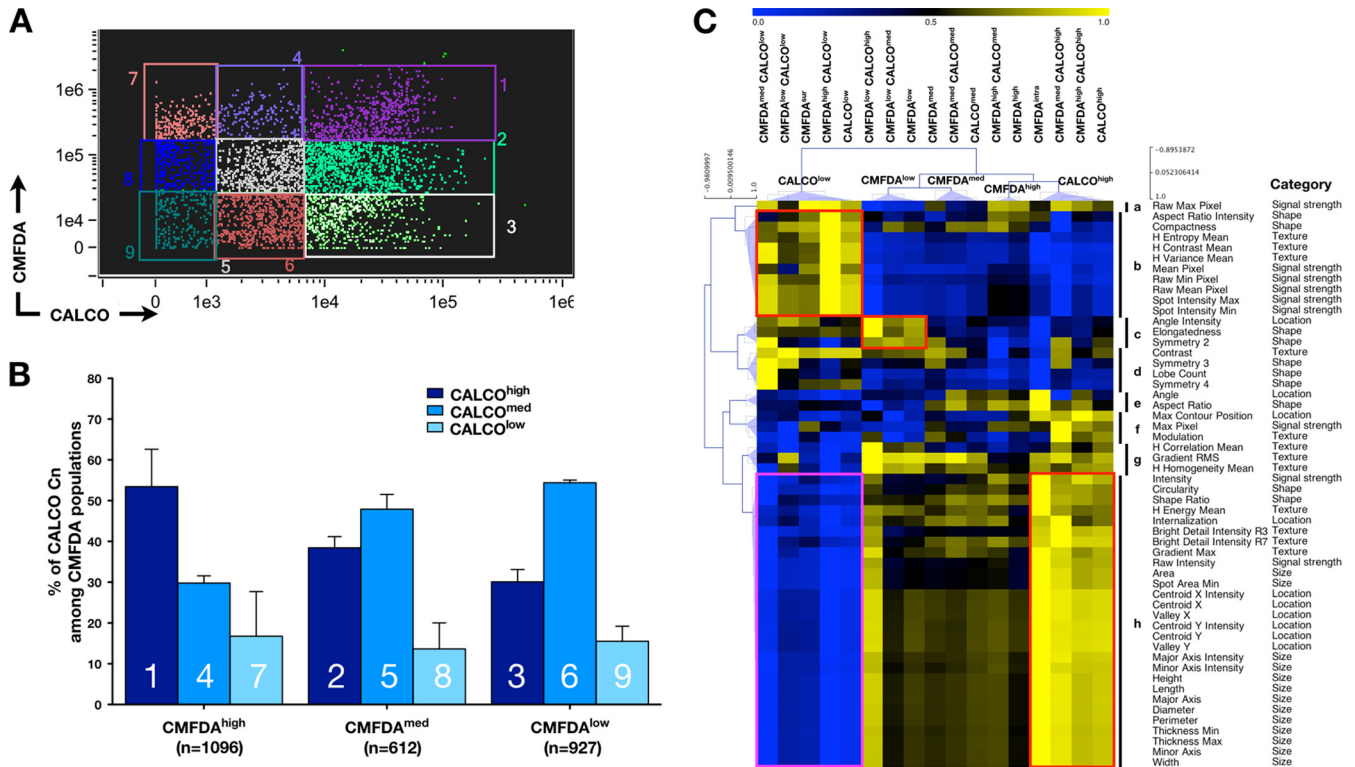
FIG 4 Multispectral imaging flow cytometry confirms the heterogeneity of the *C. neoformans* populations in the lungs of outbred OF1 mice. *C. neoformans* from the pooled lungs of 14 mice (a total of 2,635 yeast cells) were analyzed for multiplication, stress response, and viability. (A) Nine H99 populations (1 to 9) were delineated by multispectral imaging flow cytometry (Imagestream^X). The nine gates were adjusted on the basis of optical control of the fluorescence intensity of the corresponding pictured events. One representative of two independent experiments is shown. (B) The distribution of the CALCO populations (high, medium, and low) in the different CMFDA population is shown. Bars represent the means ± the standard deviations of the nine populations, with numbers corresponding to those shown in panel A. The CALCO^{low} population always represented <20%. In the CMFDA^{high} population, the CALCO^{high} population was predominant, whereas the CALCO^{med} population was predominant in the CMFDA^{med} and CMFDA^{low} populations. (C) Heat map generated from the BF channel pictures on the basis of the geometric mean of 54 different algorithms. Five groups of yeast cells composed mainly of CALCO^{low}, CALCO^{high} CMFDA^{high}, CMFDA^{med}, CMFDA^{low}, and eight groups (a to h) of algorithms clustered. Cluster h, which includes all of the size and most of the location algorithms, delineated the CALCO^{high} (yellow, red outline) and CALCO^{low} (blue, pink outline) populations, indicating that the CALCO^{high} cells consisted mostly of big yeast cells and the CALCO^{low} cells consisted mostly of small yeast cells. Cluster b distinguished CALCO^{low} cells from the other four populations as having a specific signal strength and texture (higher value of the corresponding algorithms, red outline). Cluster c distinguished CMFDA^{low} cells from the other four populations on the basis of some shape and location algorithms (higher value of the corresponding algorithms, red outline).

precise knowledge on their site of residence. We focused here on the lung because it was the only body site where well-delineated populations composed of enough yeast cells to allow further analysis were observed.

We assumed that dormant cells would be metabolically poorly active. The population that met this criterion was the CMFDA^{low} population that included less than 20% of the dead yeast (drop *C. neoformans*) cells. The delayed or absent growth of the CMFDA^{low} population undergoing serum starvation (YPD) was partially rescued by the addition of FCS, a phenotype described for dormant cells of various origins (mammalian fibroblasts, mammalian cancer cells, stem cells, bacteria, and *S. cerevisiae*) (62). This suggested that the CMFDA^{low} population could be composed predominantly of dormant cells.

Zaragoza and Nielsen evoked the possible role of their titan cells in dormancy (63). It is interesting that, in our studies, the biggest cells corresponding most probably to titan cells were composed almost exclusively of mother cells in the lungs (see Fig. S3D in the supplemental material), confirming data obtained from *in vitro* culture (23). Titan cells are composed of the three CMFDA

populations, thus suggesting that some of them (CMFDA^{low}) could be dormant. The original report on the multiplication of titan cells under standard culture conditions (Sabouraud agar plates) without the need for additional growth factors (23) does not contradict this finding since the titan cells were not sorted on CMFDA fluorescence.

The limited number of cells after sorting (Table 1) led us to implement a transcriptional gene analysis based on the adaptation of single-cell PCR assays. We were not able to analyze the expression of all of the genes in the mice_CMFDA^{low} cells because of the limited number of cells recovered from lungs. However, the finding that a cluster of genes (C1, Fig. 8) known to be overexpressed during lung infection (21) was upregulated only in yeast cells recovered from lungs (mice_CMFDA^{med}, mice_CMFDA^{high}) was a means to validate the technical and biological approach. The major difference between the CMFDA^{low} population and the other populations, whatever the condition, was modulated expression of the *PCK1* (decrease) and *COX1* (increase) genes. The phosphoenolpyruvate carboxykinase 1 (Pck1) protein plays a major role in gluconeogenesis, which is known to impact yeast cell sur-
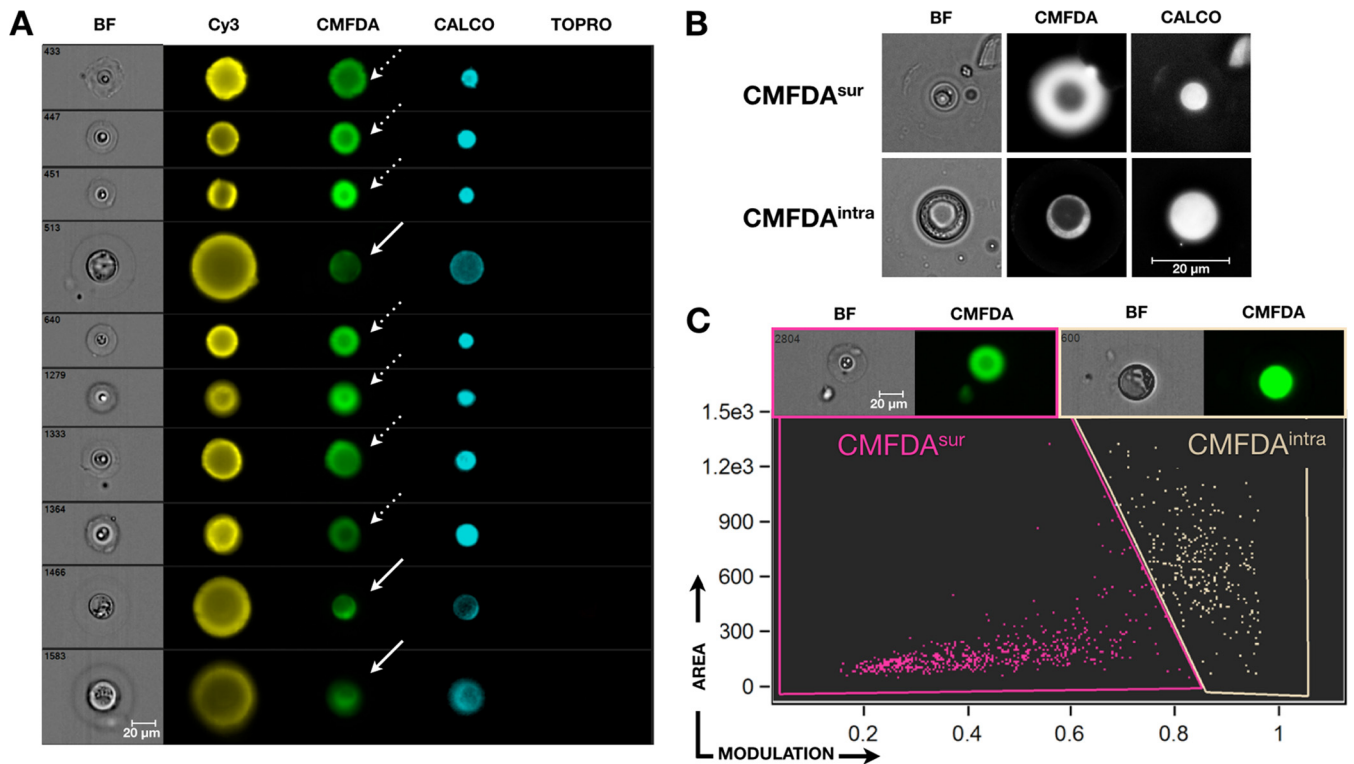
FIG 5 Morphological and fluorescence features of the Calco^high/CMFDA^high H99 population in the lungs of outbred OF1 mice. (A) Multispectral imaging flow cytometry (Imagestream^X; Amnis) was used to picture each event of the CALCO^high/CMFDA^high population in five channels: BF (transmitted light), yellow (Cy3, capsule), green (CMFDA, stress response), blue (CALCO, multiplication), and red (TOPRO, viability). Different patterns of morphology and CMFDA fluorescence were observed. (B) The CALCO^high CMFDA^high population of yeast cells from lung homogenates was also observed by classical fluorescence microscopy. CMFDA fluorescence was observed surrounding the cell wall CMFDA^sur (white dotted arrows in panel A), or within the yeast cell cytoplasm (CMFDA^intra, white arrows in panel A). (C) Multispectral imaging flow cytometry based on the modulation algorithm (texture) and the area (size) of the yeast cells easily discriminated CMFDA^intra and CMFDA^sur cells. The CMFDA^sur yeast cells were composed of regular and drop *C. neoformans* cells.

vival (64). Decreased *PCK1* expression (macrophage_CMFDA^low and mice_CMFDA^low) was associated with increased expression of *ATG9* and *VPS13* (genes involved in autophagy [65, 66]) (macrophage_CMFDA^low), suggesting that the CMFDA^low population may not need activation of the gluconeogenesis pathway and could use autophagy to survive starvation. Toffaletti et al. suggested that *COX1* (encoding mitochondrial cytochrome *c* oxidase subunit 1) was upregulated during the stress response induced by high temperature (39°C) (67) and differentially expressed in well-characterized clinical isolates in correlation with intramacrophagic proliferation (19). In *C. neoformans*, mutations in various mitochondrial genes affect the respiration rate, the response to oxidative stresses, and the ability to survive low-oxygen conditions (68, 69), and this independently of glutathione activity. In *C. gattii*, enhanced mitochondrial activity and modifications of mitochondrial morphology were found to be related to an increased proliferation rate and increased virulence (41, 70). *COX1* upregulation in the CMFDA^low population (glutathione-dependent stress response) could reflect increased mitochondrial activity that could contribute to maintenance of viability in hostile environments.

Finally, the proof of concept described herein needs to be translated to *in vitro* assays to generate large quantities of these low stress responder yeast cells. A basic description of dormancy would then be possible.

MATERIALS AND METHODS

***C. neoformans* strains and cell line.** *C. neoformans* strain H99 (serotype A, *MATα*, haploid; kindly donated by J. Heitman, Duke University, Durham, NC) was used as the reference in all of our experiments (71). Two *C. neoformans* clinical isolates (AD1-83a and AD1-07a, serotype A, *MATα*) were selected on the basis of their virulence characteristics (19). They were previously recovered from the cerebrospinal fluid of patients enrolled in the CryptoA/D study (31) and werer responsible for single infections (one isolate/one genotype/one infection). Before each experiment, yeast cells were first cultured on Sabouraud agar medium and then subcultured in 10 ml of liquid YPD at 30°C at 150 rpm for 22 h (standard YPD culture).

The J774.16 cell line (J774; American Type Culture Collection) was used to study the interaction of *C. neoformans* isolates with macrophages. Cells were maintained at 37°C in the presence of 5% CO_2 in Dulbecco's modified Eagle's medium (DMEM) supplemented with 10% heat-inactivated FCS and 1% penicillin/streptomycin (fresh medium) (all from Invitrogen). Cells were used between 10 and 35 passages.

Reagents and *C. neoformans* labeling. The white dye CALCO (Fluorescent brightener 28; Sigma) was used to monitor yeast multiplication. Staining was performed before incubation with macrophages (19) or inoculation into mice. TOPRO (Invitrogen) diluted to 10 μM in phosphate-buffered saline (PBS) was used to stain nucleic acids of cells with a disrupted membrane (dead yeast cells) and then analyzed in the allophycocyanin (APC) channel. CMFDA (CellTracker Green CMFDA; Life Technologies) is a dye that needs two enzymatic steps and glutathione to acquire fluorescence properties (fluorescein isothiocyanate [FITC]
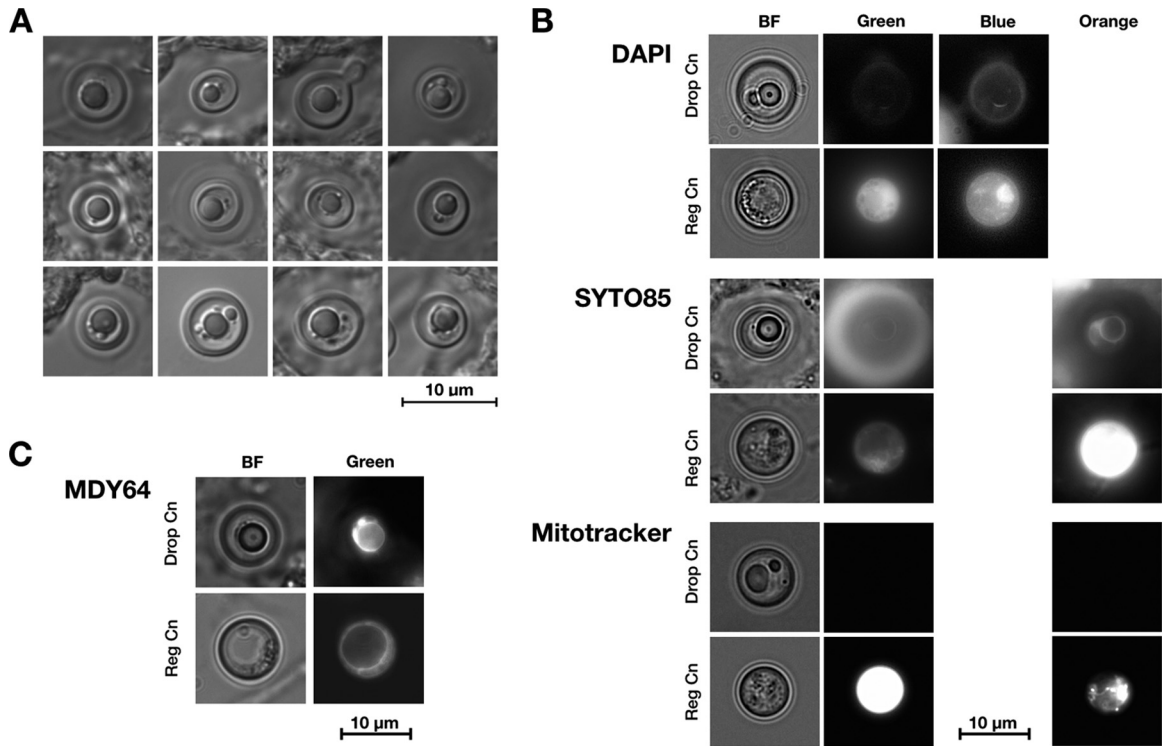
FIG 6 Morphological features and metabolic activity revealed that the drop *C. neoformans* (Drop Cn) cells in the lungs of outbred OF1 mice were dead yeast cells. Yeast cells from lung homogenates were observed by interference contrast microscopy. (A) Examples of cells composing a subpopulation of yeast cells with a typical morphology (small size [$5.80 \pm 0.80\ \mu$m, $n = 12$], thick cell wall, and one well-defined round refrigent vesicle) are shown. (B) Nucleus morphology (DAPI, blue), RNA content (SYTO85, orange), and mitochondrial activity (Mitotracker, orange) were assessed in yeast cells previously stained with CMFDA (green). Drop *C. neoformans* cells were devoid of nucleus (regular shape and regular DAPI fluorescence), RNA, and mitochondrial activities, in contrast to regular *C. neoformans* (Reg Cn) cells. (C) Lipid membrane layers (MDY64, green) were assessed in unstained yeast cells. Drop *C. neoformans* cells harbored a complete retraction of the cytoplasm around the central refrigent vesicle.

channel). It is commonly used to quantify glutathione in mammalian cells (56, 57) and has been employed for long-term tracking of *C. neoformans in vivo* (59). The stock solution in anhydrous dimethyl sulfoxide was diluted to 10 μM in PBS. Preliminary experiments showed that combining TO-PRO and CMFDA for 30 min of incubation at 37°C without agitation was efficient at *C. neoformans* concentrations ranging from 10^6 to 10^7 cells/ml and in the presence of tissue debris. CALCO staining was always performed with living cells prior to the use of all other stimuli, whereas the CMFDA/TOPRO assay followed them. The various dyes did not alter yeast cell viability (data not shown).

In specific experiments, yeast cells were subjected *in vitro* to various stimuli to test the glutathione-mediated stress response, washed twice, and then subjected to the CMFDA/TOPRO assay at different time points. The stimuli included (i) pure water; (ii) hydrogen peroxide (Sigma) adjusted to 2 mM in water (72); (iii) fresh medium or YNB, which represents a nonoptimal culture medium for yeast cells on the basis of preliminary experiments (data not shown); (iv) heating at 65°C for 2 h, which killed 99.9% of the yeast cells. All stimuli were tested in duplicate. Diethyl maleate (Sigma) adjusted to 100 μM in sterile water was used to deplete the *C. neoformans* glutathione stock (56) and assess glutathione-dependent CMFDA staining.

E1, a murine IgG1 anti-capsular polysaccharide monoclonal antibody (MAb) was used as an opsonin (73). Polyclonal rabbit anti-capsular antibodies together with cyanine 3 (Cy3) or R-phycoerythrin (PE)-labeled goat anti-rabbit IgG (anti-IgG–Cy3 or anti-IgG–PE) (Invitrogen) were used to stain the capsule of *C. neoformans* at 1:100 for 30 min of incubation. The polyclonal sera were obtained by a method of immunization of rabbits with whole heat-killed *C. neoformans* cells adapted from published procedures (74). Additional dyes were used as follows to characterize

metabolic activities or yeast cell organization: (i) mitochondrial activity with Mitotracker Orange CMTMRos (Invitrogen) at 40 nM (30 min of incubation at 37°C) (41), (ii) RNA content with SYTO85 (Invitrogen) at 5 μM (30 min of incubation at 37°C), (iii) lipid membrane layer staining with MDY64 (Invitrogen) at 10 μM (3 min of incubation at room temperature [RT]) (23), and (iv) nucleus morphology with DAPI (Invitrogen) at 1:5,000 (5 min of incubation at RT) (23).

***In vitro* and *in vivo* models to study yeast host adaptation. (i) Fungal cell isolation after *C. neoformans*-macrophage interaction.** J774 cell suspension (10^5 cells in fresh medium per well of a 24-well culture plate) were incubated at 37°C in 5% CO_2 for 48 h. On the day of the experiment, an E1 MAb- and CALCO-stained *C. neoformans* suspensions, both in fresh medium at the desired concentrations, were added to the J774 cell monolayer and incubated at 37°C and 5% CO_2 for 2 h (*C. neoformans*/J774 ratio of 5:1). Nonadherent extracellular yeast cells were then removed by washings with PBS, and incubation was stopped (iH2) or protracted for 24 h (iH24). At the end of the incubation time, nonadherent yeast cells were removed by washing with PBS and intracellular yeast cells were recovered with a cell scrapper and 0.05% sodium dodecyl sulfate (Sigma) in ice-cold RNase-free water (Invitrogen) (lysis solution) over the macrophage layer. The yeast cell suspension was then centrifuged and washed twice with PBS.

(ii) Fungal cell isolation from organs of infected mice. Experimental infections were performed with 6- to 8-week-old outbred OF1 (Charles Rivers Laboratories) or BALB/c (Janvier Labs) male mice.

The inoculum was prepared in sterile saline from CALCO-stained yeast cells after standard YPD culture. A 10^6-cell/ml *C. neoformans* suspension was inoculated intravenously (10^5 cells/mouse). For specific experiments, mice were sacrificed at early time points (30 min and 7, 15, and
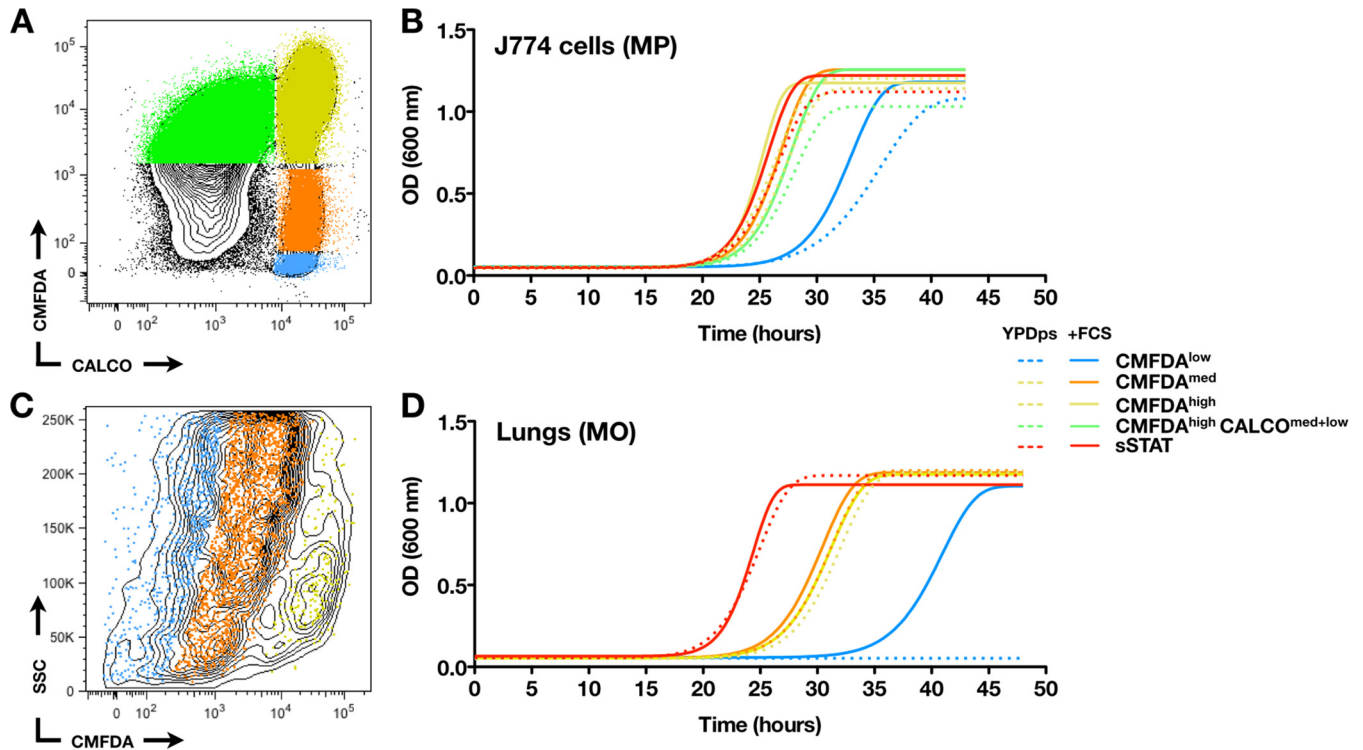
FIG 7 Analysis of the growth curves of different CMFDA populations after sorting. Yeast cells recovered from macrophage lysis (MP) after 24 h of interaction (A and B) or lung homogenates (MO) from infected outbred mice (C and D) were stained and then sorted (FACSAria II; BD). Stationary-phase yeast cells stained at the same time (sSTAT, red) were used as a control. Yeast cells (10^4/ml) of each population were allowed to grow in YPDps (dashed lines) or YPDps plus 10% FCS (+FCS, solid lines) in the wells of a 96-well plate at 30°C with agitation (800 rpm). The OD_{600} was recorded over time. (A) Four CMFDA populations (CMFDA/CALCO dot plot) were studied: CMFDA^{high} CALCO^{high} (yellow), CMFDA^{med} CALCO^{high} (orange) CMFDA^{low} CALCO^{high} (blue) and CMFDA^{high} CALCO$^{med+low}$ (green). (B) The exponential growth phase of the CMFDA^{low} population (blue) was delayed compared to that of the other three populations and sSTAT. Onset of the exponential phase occurred earlier with the addition of FCS. (C) Three CMFDA populations (CMFDA SSC dot plot) of yeast cells recovered from pooled lung homogenates were analyzed: CMFDA^{high} (yellow), CMFDA^{med} (orange), and CMFDA^{low} (blue). (D) The CMFDA^{low} population (blue) failed to grow in YPD even after 48 h of incubation. Addition of FCS restored growth capacities even though onset was delayed by $\geq$10 h compared to that of the other populations and sSTAT. In addition, growth of CMFDA^{high} and CMFDA^{med} populations was similar and delayed compared to that of sSTAT.

30 h) after inoculation. After sacrifice, the lungs, spleen, and brain were aseptically removed. Tissues were then homogenized by grinding with a Potter homogenizer with 2 ml of lysis solution. The suspension was transferred into a 2-ml tube, centrifuged at a relative centrifugal force (RCF) of 2,000, and washed twice with lysis solution and once with PBS. The pellet was then filtered with a 40-μm cell strainer (BD Biosciences) in PBS over a sterile petri dish to remove the largest tissue debris. The filtrate was then centrifuged and washed once with PBS.

(iii) Stress response staining protocol (CMFDA/TOPRO assay). After the yeast cell pellet was washed, a solution of CMFDA (10 μM) and TOPRO (10 μM) in PBS was added and the mixture incubated for 30 min at 37°C. Three washings with PBS were then performed to remove extra dyes. For specific experiments, the pellet was then incubated for 30 min at RT in a 1:100 solution of polyclonal rabbit anticapsular antibodies together with anti-IgG–Cy3 or anti-IgG–PE and washed twice in PBS. Just before flow cytometry analysis, an additional filtration step (35-μm cell strainer) was performed to remove newly formed aggregates.

Analysis of *C. neoformans* populations upon host interaction. (i) Microscopy techniques. Interferential contrast microscopy (DM LB2 microscope; Leica) and epifluorescence microscopy (Axio Scan; Carl Zeiss) were used to analyze the morphology and fluorescence features of yeast cells recovered from lung homogenates before and after staining and pictured with an AxioCam MRm camera (Carl Zeiss).

Yeast multiplication was assessed by dynamic imaging (Nikon Biostation). Yeast cells recovered from lung homogenates were suspended in YPD at 30°C without CO_2. Series of images were taken by phase contrast

and fluorescence microscopy (DAPI filter) every 10 min for 48 h at ×40 magnification.

(ii) Classical flow cytometry analysis. To better characterize yeast cell populations in terms of multiplication and stress responses, fluorescence intensity was quantified with a MacsQuant Analyzer with the MacsQuantify Software 2.0 (Miltenyi Biotec) and analyzed with FlowJo 8.7 software (Tree Star, Inc.). Aggregates were excluded by gating relevant events in the forward scatter/side scatter (FSC/SSC) contour plot. PE^{high} (yeast cells) and APC^{low} (viable yeast cells) populations were then gated, and the DAPI/FITC channel dot plot was analyzed for multiplication (CALCO/DAPI channel) and stress responses (CMFDA/FITC channel).

(iii) Multispectral flow cytometry analysis. To connect cell morphology and fluorescence features we used Imagestream^X with the INSPIRE software (Amnis Corporation). Suspensions were adjusted to 10^7 cells in 80 μl, and 10,000 cells were recorded at ×40 magnification in five different channels, including the bright-field (BF) channel and four fluorescence channels (channel 3, 560 to 595 nm [E1-Cy3, yeast cells]; channel 2, 470 to 560 nm [CMFDA]; channel 7, 430 to 505 nm [CALCO]; channel 11, 660 to 720 nm [TOPRO]). Data analysis was performed with the IDEAS software (Amnis Corporation) after fluorescence compensation procedures. The first step was the definition of a mask that delineated the relevant pixels in each picture. Fifty-four algorithms (calculations made for each event within a defined mask) were then available to analyze size, texture, location, shape, or signal strength.

Using basic algorithms, unfocused events, tissue debris, yeast cell aggregates, and dead yeast cells were excluded (see Fig. S2 in the supplemen-
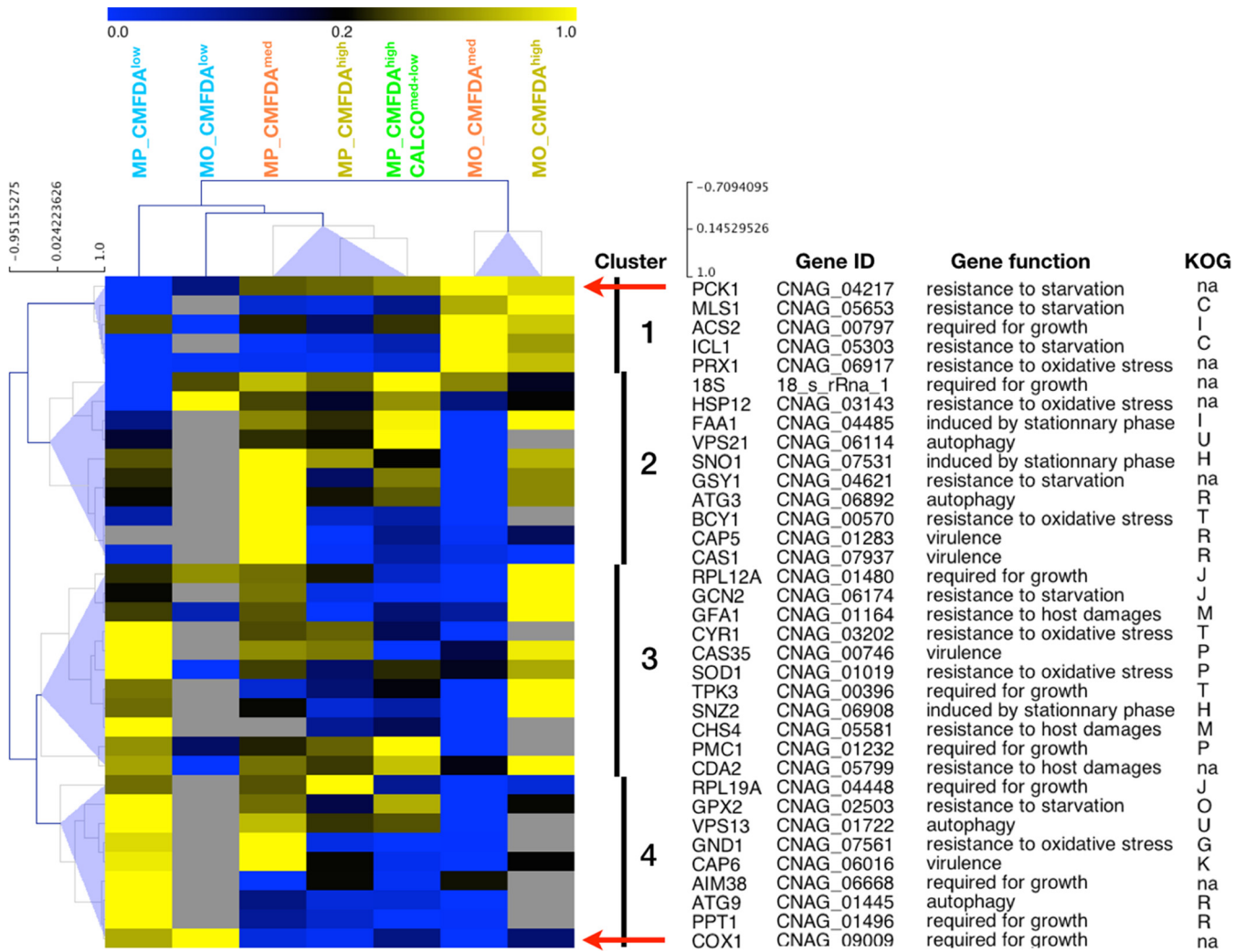
FIG 8 Heat map of gene expression analysis (*n* = 37) of different CMFDA populations by real-time quantitative PCR. CMFDA populations of yeast cells recovered from macrophages (MP) or murine lungs (MO) were studied. After lyophilization, yeast cells were lysed and primer-specific reverse transcription and quantitative PCR were performed. The targets selected (*n* = 37) were genes involved in growth, stationary phase, resistance to oxidative stress, autophagy, adaptation to the lung environment, and capsule and chitin formation. For each gene, the fold change compared to the *ACT1* and *GAPDH* genes was normalized between 0 and 1. The genes for which amplification failed are depicted in grey. MO_CMFDA^med and MO_CMFDA^high from mice clustered together with each other and apart from the other populations. All of the macrophage populations except MP_CMFDA^low clustered together. The pattern of expression of MP_CMFDA^low and MO_CMFDA^low was different from that of the other populations and between them, except for *PCK1* and *COX1* (red arrows). Four clusters of genes can be differentiated, with C1 specifically composed of genes involved in lung adaptation during infection (21) and C4 composed of genes expressed more in the MP_CMFDA^low population.

TABLE 1 Distribution of the various CMFDA populations studied after 24 h of macrophage interaction and in lungs of infected outbred mice

| | Mean no. of yeast cells (10^5) ± SD[a] for analysis of: | | | |
| | Growth curves | | Gene expression | |
Population	Macrophages	Lung homogenate	Macrophages	Lung homogenate
CMFDA^low	5.8 ± 0.1	0.7 ± 0.2	8 ± 1.6	1.1 ± 0.6
CMFDA^med	12.8 ± 2.5	2.5 ± 1.5	17.4 ± 2.1	4.6 ± 0.3
CMFDA^high	38.8 ± 3.9	0.6 ± 0.2	26.5 ± 0.7	0.9 ± 0.1
CMFDA^high CALCO^low	27.0 ± 7.1	ND[b]	27.5 ± 3.5	ND

[a] Two independent experiments were performed with macrophages and lung homogenates (21 and 42 pooled lungs recovered 7 days after inoculation).
[b] ND, not done.

tal material). For multiplication and stress response analyses, gates were determined on the basis of the CALCO/CMFDA dot plot considering the intensity algorithm and optical control of the events pictured in the gates. For each population of interest, the geometric mean was calculated with the IDEAS software. From the whole data set and each algorithm, data were then normalized between 0 and 1, with 0 as the minimal value and 1 as the maximal value. Schematic representation was performed with the open-source genomic analysis software MeV v4.6.1 (The TM4 Development Group) obtained from http://www.tm4.org (75). Hierarchical clustering was performed by complete linkage clustering and Pearson correlation.

Analysis of specific *C. neoformans* populations. (i) Sorting of the *C. neoformans* cell population on the basis of CMFDA fluorescence intensity. On the basis of the discovery of variable *C. neoformans* stress responses upon host interaction, cell sorting was used to better characterize the phenotypes of these populations with the FACS Aria II (BD Biosciences).

Yeast cells obtained after 24 h of incubation with macrophages were sorted on the basis of the CALCO/CMFDA dot plot while yeast cells obtained from 21 to 42 mice inoculated 7 days before were sorted on the basis of the SSC/CMFDA dot plot. Aggregates, cell debris (PE[low] population), and dead yeast cells (APC[high] population) were then excluded. Three populations were sorted as CMFDA[high], CMFDA[medium], and CMFDA[low] for both conditions, with an additional population of CMFDA[high] CALCO[med+low] for the yeast cells recovered after macrophage interaction (Fig. 7A and C). The purity of each sorted population was assessed by fluorescence microscopy (see Fig. S6 in the supplemental material) Independent duplicate experiments were performed and used for determination of growth kinetics and gene expression analysis.

A yeast cell sample harvested from a standard YPD culture, stained at the same time, and stored under the same conditions as the experimental samples was used as a control (control yeast cells).

(ii) Growth curves determination. The growth kinetics of each population were analyzed. After sorting and centrifugation at an RCF of 2,000, the populations were resuspended in sterile YPD containing 10% penicillin/streptomycin (YPDps) at the desired concentration on the basis of the absolute count provided by the cell sorter.

Each sample was studied in duplicate in the presence or absence of 10% FCS supplementation (100-μl final volume) in parallel with control yeast cells and medium alone. The plates were incubated in a ThermoMixer at 30°C and 700 rpm. Optical density at 600 nm (OD_{600}) was recorded at different time points. Analysis of the growth curves was performed with Prism Software 5.0 (GraphPad Software) and the Weibull algorithm (76).

(iii) Sample preparation for quantitative real-time PCR. After sorting, the different *C. neoformans* populations were washed carefully in RNase-free water to remove PBS salts, flash-frozen in liquid nitrogen, and stored at −80°C. Control yeast cells cultured in YPD medium were processed in parallel. All experiments were performed with the SuperScript III Platinum CellsDirect One-Step quantitative reverse transcription-PCR kit (Invitrogen), which is classically used for single-cell PCR analyses. The day before RNA extraction, the samples were lyophilized overnight. One microliter of lysis enhancer and 10 μl of resuspension buffer were added to the lyophilized samples and incubated 10 min at 75°C. A 1.6-μl volume of DNase buffer and a 5-μl volume of DNase I were then added, and the mixture was incubated for 5 min at 25°C and then inactivated with 4 μl of EDTA and incubation at 70°C for 10 min. RNA samples were then stored at −80°C.

(iv) Quantitative real-time PCR. We based our selection on the genes that were homologues between H99 and *S. cerevisiae* (77). All H99 genes for which the *S. cerevisiae* gene description contained the keywords growth, stationary phase, starvation, and oxidative stress were first selected. Additional H99 genes involved in capsule and cell wall formation and some regulated during early pulmonary infection (21) were added (see Table S1 in the supplemental material). The coding sequence of the selected H99 genes was then retrieved from the Broad Institute website

(http://www.broadinstitute.org/annotation/genome/cryptococcus_neoformans/MultiHome.html). The sequences of 90 different predesigned locked nucleic acids octamer probes of the human Universal ProbeLibrary set (Roche) were used as the probe library. If a probe matched the selected gene, the corresponding primers were designed with the dedicated ProbeFinder Software (Roche Universal ProbeLibrary). At the end, 37 assays (see Table S2) were implemented for real-time quantitative PCR, including 33 for nuclear genes, 1 for a ribosomal RNA gene (18S rRNA), 1 for a mitochondrial gene (*COX1*), and 2 for reference genes (*ACT1* and *GAPDH*).

Quantitative reverse transcription-PCR that allows primer-specific reverse transcription (50°C for 15 min) and quantitative PCR amplification on the basis of probe detection (95°C for 2 min and 45 cycles of 95°C for 15 s and 60°C for 30 s) was performed in a total volume of 10 μl including 2 μl of a 1:10 dilution of each RNA samples.

Each RNA sample was normalized with the geometric mean of the quantification cycle of the corresponding *ACT1* and *GAPDH* gene expression (78). Fold changes for each sample were calculated according to Pfaffl (79). For hierarchical clustering analysis with MeV v4.6.1, the data were normalized as described above.

Ethics statements. This study was carried out in strict accordance with the French and European regulations on the care and protection of laboratory animals (EC directive 86/609, French law 2001-486 issued on 6 June 2001). Animals were housed at the Institut Pasteur animal facilities, which are accredited by the French Ministry of Agriculture to perform experiments with live mice (accreditations A 75 15-27 and B 75 15-05, issued on 12 November 2004 and 22 May 2008, respectively). The protocol was approved by the Institut Pasteur Animal Care Committee (number 03/144) and performed in compliance with the NIH Animal Welfare Insurance (number a5476-01 issued on 2/7/2007). All efforts were made to minimize suffering during animal handling and experimentation. Animals were housed seven per cage in our animal facilities and received food and water *ad libitum*. Mice were euthanized by CO_2 inhalation.

SUPPLEMENTAL MATERIAL

Supplemental material for this article may be found at http://mbio.asm.org/lookup/suppl/doi:10.1128/mBio.02580-14/-/DCSupplemental.

Figure S1, PDF file, 0.1 MB.
Figure S2, PDF file, 0.8 MB.
Figure S3, PDF file, 0.2 MB.
Figure S4, PDF file, 0.1 MB.
Figure S5, PDF file, 0.2 MB.
Figure S6, PDF file, 0.9 MB.
Figure S7, PDF file, 0.2 MB.
Table S1, XLSX file, 0.1 MB.
Table S2, XLSX file, 0.02 MB.

REFERENCES

1. **Casadevall A, Steenbergen JN, Nosanchuk JD.** 2003. "Ready made" virulence and "dual use" virulence factors in pathogenic environmental fungi—the *Cryptococcus neoformans* paradigm. Curr Opin Microbiol **6:**332–337. http://dx.doi.org/10.1016/S1369-5274(03)00082-1.
2. **Steenbergen JN, Shuman HA, Casadevall A.** 2001. *Cryptococcus neoformans* interactions with amoebae suggest an explanation for its virulence and intracellular pathogenic strategy in macrophages. Proc Natl Acad Sci U S A **98:**15245–15250. http://dx.doi.org/10.1073/pnas.261418798.
3. **Derengowski Lda S, Paes HC, Albuquerque P, Tavares AH, Fernandes L, Silva-Pereira I, Casadevall A.** 2013. The transcriptional response of *Cryptococcus neoformans* to ingestion by *Acanthamoeba castellanii* and macrophages provides insights into the evolutionary adaptation to the

mammalian host. Eukaryot Cell **12**:761–774. http://dx.doi.org/10.1128/EC.00073-13.

4. **Frager SZ, Chrisman CJ, Shakked R, Casadevall A**. 2010. *Paramecium* species ingest and kill the cells of the human pathogenic fungus *Cryptococcus neoformans*. Med Mycol **48**:775–779. http://dx.doi.org/10.3109/13693780903451810.

5. **Fries BC, Taborda CP, Serfass E, Casadevall A**. 2001. Phenotypic switching of *Cryptococcus neoformans* occurs in vivo and influences the outcome of infection. J Clin Invest **108**:1639–1648. http://dx.doi.org/10.1172/JCI13407.

6. **García-Rodas R, Zaragoza O**. 2012. Catch me if you can: phagocytosis and killing avoidance by *Cryptococcus neoformans*. FEMS Immunol Med Microbiol **64**:147–161. http://dx.doi.org/10.1111/j.1574-695X.2011.00871.x.

7. **Charlier C, Nielsen K, Daou S, Brigitte M, Chretien F, Dromer F**. 2009. Evidence of a role for monocytes in dissemination and brain invasion by *Cryptococcus neoformans*. Infect Immun **77**:120–127. http://dx.doi.org/10.1128/IAI.01065-08.

8. **Santangelo R, Zoellner H, Sorrell T, Wilson C, Donald C, Djordjevic J, Shounan Y, Wright L**. 2004. Role of extracellular phospholipases and mononuclear phagocytes in dissemination of cryptococcosis in a murine model. Infect Immun **72**:2229–2239. http://dx.doi.org/10.1128/IAI.72.4.2229-2239.2004.

9. **Kronstad JW, Attarian R, Cadieux B, Choi J, D'Souza CA, Griffiths EJ, Geddes JM, Hu G, Jung WH, Kretschmer M, Saikia S, Wang J**. 2011. Expanding fungal pathogenesis: *Cryptococcus* breaks out of the opportunistic box. Nat Rev Microbiol **9**:193–203. http://dx.doi.org/10.1038/nrmicro2522.

10. **Goldman DL, Khine H, Abadi J, Lindenberg DJ, Pirofski La, Niang R, Casadevall A**. 2001. Serologic evidence for *Cryptococcus neoformans* infection in early childhood. Pediatrics **107**:E66. http://dx.doi.org/10.1542/peds.107.5.e66.

11. **Baker RD**. 1976. The primary pulmonary lymph node complex of cryptococcosis. Am J Clin Pathol **65**:83–92.

12. **Garcia-Hermoso D, Janbon G, Dromer F**. 1999. Epidemiological evidence for dormant *Cryptococcus neoformans* infection. J Clin Microbiol **37**:3204–3209.

13. **Dromer F, Ronin O, Dupont B**. 1992. Isolation of *Cryptococcus neoformans* var. *gattii* from an Asian patient in France: evidence for dormant infection in healthy subjects. J Med Vet Mycol **30**:395–397. http://dx.doi.org/10.1080/02681219280000511.

14. **Dromer F, Casadevall A, Perfect J, Sorrell T**. 2010. *Cryptococcus neoformans*: latency and disease, p 429. In Heitman J, Kozel TR, Kwon-Chung KJ, Perfect JR, Casadevall A (ed), *Cryptococcus*: from human pathogen to model yeast. ASM Press, Washington, DC.

15. **Eisenman HC, Casadevall A, McClelland EE**. 2007. New insights on the pathogenesis of invasive *Cryptococcus neoformans* infection. Curr Infect Dis Rep **9**:457–464. http://dx.doi.org/10.1007/s11908-007-0070-8.

16. **Chrétien F, Lortholary O, Kansau I, Neuville S, Gray F, Dromer F**. 2002. Pathogenesis of cerebral *Cryptococcus neoformans* infection after fungemia. J Infect Dis **186**:522–530. http://dx.doi.org/10.1086/341564.

17. **French N, Gray K, Watera C, Nakiyingi J, Lugada E, Moore M, Lalloo D, Whitworth JA, Gilks CF**. 2002. Cryptococcal infection in a cohort of HIV-1-infected Ugandan adults. AIDS **16**:1031–1038. http://dx.doi.org/10.1097/00002030-200205030-00009.

18. **Olszewski MA, Zhang Y, Huffnagle GB**. 2010. Mechanisms of cryptococcal virulence and persistence. Future Microbiol **5**:1269–1288. http://dx.doi.org/10.2217/fmb.10.93.

19. **Alanio A, Desnos-Ollivier M, Dromer F**. 2011. Dynamics of *Cryptococcus neoformans*-macrophage interactions reveal that fungal background influences outcome during cryptococcal meningoencephalitis in humans. mBio **2**:e00158–11. http://dx.doi.org/10.1128/mBio.00158-11.

20. **Feldmesser M, Kress Y, Novikoff P, Casadevall A**. 2000. *Cryptococcus neoformans* is a facultative intracellular pathogen in murine pulmonary infection. Infect Immun **68**:4225–4237. http://dx.doi.org/10.1128/IAI.68.7.4225-4237.2000.

21. **Hu G, Cheng P-Y, Sham A, Perfect JR, Kronstad JW**. 2008. Metabolic adaptation in *Cryptococcus neoformans* during early murine pulmonary infection. Mol Microbiol **69**:1456–1475. http://dx.doi.org/10.1111/j.1365-2958.2008.06374.x.

22. **Okagaki LH, Strain AK, Nielsen JN, Charlier C, Baltes NJ, Chrétien F, Heitman J, Dromer F, Nielsen K**. 2010. Cryptococcal cell morphology

23. **Zaragoza O, García-Rodas R, Nosanchuk JD, Cuenca-Estrella M, Rodríguez-Tudela JL, Casadevall A**. 2010. Fungal cell gigantism during mammalian infection. PLoS Pathog **6**:e1000945. http://dx.doi.org/10.1371/journal.ppat.1000945.

24. **Crabtree JN, Okagaki LH, Wiesner DL, Strain AK, Nielsen JN, Nielsen K**. 2012. Titan cell production enhances the virulence of *Cryptococcus neoformans*. Infect Immun **80**:3776–3785. http://dx.doi.org/10.1128/IAI.00507-12.

25. **Lortholary O, Improvisi L, Nicolas M, Provost F, Dupont B, Dromer F**. 1999. Fungemia during murine cryptococcosis sheds some light on pathophysiology. Med Mycol **37**:169–174. http://dx.doi.org/10.1080/j.1365-280X.1999.00215.x.

26. **Neuville S, Lortholary O, Dromer F**. 2000. Do kinetics of the humoral response to *Cryptococcus neoformans* proteins during murine cryptococcosis reflect outcome? Infect Immun **68**:3724–3726. http://dx.doi.org/10.1128/IAI.68.6.3724-3726.2000.

27. **Clemons KV, Stevens DA**. 2010. Cryptococcosis in experimental animals: lessons learned, p 473–488. In Heitman J, Kozel TR, Kwon-Chung KJ, Perfect JR, Casadevall A (ed), *Cryptococcus*: from human pathogen to model yeast. ASM Press, Washington, DC.

28. **Lin X, Heitman J**. 2006. The biology of the *Cryptococcus neoformans* species complex. Annu Rev Microbiol **60**:69–105. http://dx.doi.org/10.1146/annurev.micro.60.080805.142102.

29. **Ou X-T, Wu J-Q, Zhu L-P, Guan M, Xu B, Hu X-P, Wang X, Weng X-H**. 2011. Genotypes coding for mannose-binding lectin deficiency correlated with cryptococcal meningitis in HIV-uninfected Chinese patients. J Infect Dis **203**:1686–1691. http://dx.doi.org/10.1093/infdis/jir152.

30. **Hu X-P, Wu J-Q, Zhu L-P, Wang X, Xu B, Wang R-Y, Ou X-T, Weng X-H**. 2012. Association of Fcγ receptor IIB polymorphism with cryptococcal meningitis in HIV-uninfected Chinese patients. PLoS One **7**:e42439. http://dx.doi.org/10.1371/journal.pone.0042439.

31. **Dromer F, Mathoulin-Pélissier S, Launay O, Lortholary O, Group F**. 2007. Determinants of disease presentation and outcome during cryptococcosis: the CryptoA/D study. PLoS Med **4**:e21. http://dx.doi.org/10.1371/journal.pmed.0040021.

32. **Levitz SM, Dupont MP, Smail EH**. 1994. Direct activity of human T lymphocytes and natural killer cells against *Cryptococcus neoformans*. Infect Immun **62**:194–202.

33. **Ma LL, Wang CL, Neely GG, Epelman S, Krensky AM, Mody CH**. 2004. NK cells use perforin rather than granulysin for anticryptococcal activity. J Immunol **173**:3357–3365. http://dx.doi.org/10.4049/jimmunol.173.5.3357.

34. **Schein JE, Tangen KL, Chiu R, Shin H, Lengeler KB, MacDonald WK, Bosdet I, Heitman J, Jones SJ, Marra MA, Kronstad JW**. 2002. Physical maps for genome analysis of serotype A and D strains of the fungal pathogen *Cryptococcus neoformans*. Genome Res **12**:1445–1453. http://dx.doi.org/10.1101/gr.81002.

35. **Litvintseva AP, Mitchell TG**. 2012. Population genetic analyses reveal the African origin and strain variation of *Cryptococcus neoformans* var. *grubii*. PLoS Pathog **8**:e1002495. http://dx.doi.org/10.1371/journal.ppat.1002495.

36. **Feldmesser M, Rivera J, Kress Y, Kozel TR, Casadevall A**. 2000. Antibody interactions with the capsule of *Cryptococcus neoformans*. Infect Immun **68**:3642–3650. http://dx.doi.org/10.1128/IAI.68.6.3642-3650.2000.

37. **Garcia-Hermoso D, Dromer F, Janbon G**. 2004. *Cryptococcus neoformans* capsule structure evolution in vitro and during murine infection. Infect Immun **72**:3359–3365. http://dx.doi.org/10.1128/IAI.72.6.3359-3365.2004.

38. **Clancy CJ, Nguyen MH, Alandoerffer R, Cheng S, Iczkowski K, Richardson M, Graybill JR**. 2006. *Cryptococcus neoformans* var. *grubii* isolates recovered from persons with AIDS demonstrate a wide range of virulence during murine meningoencephalitis that correlates with the expression of certain virulence factors. Microbiology **152**:2247–2255. http://dx.doi.org/10.1099/mic.0.28798-0.

39. **Liaw S-J, Wu H-C, Hsueh PR**. 2010. Microbiological characteristics of clinical isolates of *Cryptococcus neoformans* in Taiwan: serotypes, mating types, molecular types, virulence factors, and antifungal susceptibility. Clin Microbiol Infect **16**:696–703. http://dx.doi.org/10.1111/j.1469-0691.2009.02930.x.

40. **Kozel TR, Pfrommer GS, Guerlain AS, Highison BA, Highison GJ**. 1988. Strain variation in phagocytosis of *Cryptococcus neoformans*: dissociation

affects host cell interactions and pathogenicity. PLoS Pathog **6**:e1000953. http://dx.doi.org/10.1371/journal.ppat.1000953.

of susceptibility to phagocytosis from activation and binding of opsonic fragments of C3. Infect Immun **56:**2794–2800.

41. **Ma H, Hagen F, Stekel DJ, Johnston SA, Sionov E, Falk R, Polacheck I, Boekhout T, May RC.** 2009. The fatal fungal outbreak on Vancouver Island is characterized by enhanced intracellular parasitism driven by mitochondrial regulation. Proc Natl Acad Sci U S A **106:**12980–12985. http://dx.doi.org/10.1073/pnas.0902963106.

42. **Ormerod KL, Morrow CA, Chow EW, Lee IR, Arras SD, Schirra HJ, Cox GM, Fries BC, Fraser JA.** 2013. Comparative genomics of serial isolates of *Cryptococcus neoformans* reveals gene associated with carbon utilization and virulence. G3 (Bethesda) **3:**675–686. http://dx.doi.org/10.1534/g3.113.005660.

43. **Desnos-Ollivier M, Patel S, Spaulding AR, Charlier C, Garcia-Hermoso D, Nielsen K, Dromer F.** 2010. Mixed infections and *in vivo* evolution in the human fungal pathogen *Cryptococcus neoformans*. mBio **1:**e00091-10. http://dx.doi.org/10.1128/mBio.00091-10.

44. **Charlier C, Chrétien F, Baudrimont M, Mordelet E, Lortholary O, Dromer F.** 2005. Capsule structure changes associated with *Cryptococcus neoformans* crossing of the blood-brain barrier. Am J Pathol **166:**421–432. http://dx.doi.org/10.1016/S0002-9440(10)62265-1.

45. **Steen BR, Zuyderduyn S, Toffaletti DL, Marra M, Jones SJ, Perfect JR, Kronstad J.** 2003. *Cryptococcus neoformans* gene expression during experimental cryptococcal meningitis. Eukaryot Cell **2:**1336–1349. http://dx.doi.org/10.1128/EC.2.6.1336-1349.2003.

46. **Dworkin J, Shah IM.** 2010. Exit from dormancy in microbial organisms. Nat Rev Microbiol **8:**890–896. http://dx.doi.org/10.1038/nrmicro2453.

47. **Chao MC, Rubin EJ.** 2010. Letting sleeping *dos* lie: does dormancy play a role in tuberculosis? Annu Rev Microbiol **64:**293–311. http://dx.doi.org/10.1146/annurev.micro.112408.134043.

48. **Keren I, Minami S, Rubin E, Lewis K.** 2011. Characterization and transcriptome analysis of *Mycobacterium tuberculosis* persisters. mBio **2:**e00100–11. http://dx.doi.org/10.1128/mBio.00100-11.

49. **Murphy DJ, Brown JR.** 2007. Identification of gene targets against dormant phase *Mycobacterium tuberculosis* infections. BMC Infect Dis **7:**84. http://dx.doi.org/10.1186/1471-2334-7-84.

50. **Markus MB.** 2011. The hypnozoite concept, with particular reference to malaria. Parasitol Res **108:**247–252. http://dx.doi.org/10.1007/s00436-010-2072-y.

51. **Gray JV, Petsko GA, Johnston GC, Ringe D, Singer RA, Werner-Washburne M.** 2004. "Sleeping beauty": quiescence in *Saccharomyces cerevisiae*. Microbiol Mol Biol Rev **68:**187–206. http://dx.doi.org/10.1128/MMBR.68.2.187-206.2004.

52. **Arcangioli B, Ben Hassine S.** 2009. Unrepaired oxidative DNA damage induces an ATR/ATM apoptotic-like response in quiescent fission yeast. Cell Cycle **8:**2326–2331. http://dx.doi.org/10.4161/cc.8.15.9147.

53. **Lamarre C, Sokol S, Debeaupuis J-P, Henry C, Lacroix C, Glaser P, Coppée J-Y, François J-M, Latgé J-P.** 2008. Transcriptomic analysis of the exit from dormancy of *Aspergillus fumigatus* conidia. BMC Genomics **9:**417. http://dx.doi.org/10.1186/1471-2164-9-417.

54. **Kasuga T, Townsend JP, Tian C, Gilbert LB, Mannhaupt G, Taylor JW, Glass NL.** 2005. Long-oligomer microarray profiling in *Neurospora crassa* reveals the transcriptional program underlying biochemical and physiological events of conidial germination. Nucleic Acids Res **33:**6469–6485. http://dx.doi.org/10.1093/nar/gki953.

55. **Botts MR, Hull CM.** 2010. Dueling in the lung: how *Cryptococcus* spores race the host for survival. Curr Opin Microbiol **13:**437–442. http://dx.doi.org/10.1016/j.mib.2010.05.003.

56. **Markovic J, Mora NJ, Broseta AM, Gimeno A, de-la-Concepción N, Viña J, Pallardó FV.** 2009. The depletion of nuclear glutathione impairs cell proliferation in 3t3 fibroblasts. PLoS One **4:**e6413. http://dx.doi.org/10.1371/journal.pone.0006413.

57. **Sebastià J, Cristòfol R, Martín M, Rodríguez-Farré E, Sanfeliu C.** 2003. Evaluation of fluorescent dyes for measuring intracellular glutathione content in primary cultures of human neurons and neuroblastoma SH-SY5Y. Cytometry **51:**16–25. http://dx.doi.org/10.1002/cyto.a.10003.

58. **Nishiuchi H, Tabira Y, Yamagishi K.** 2012. A combination of flow cytometry and traditional screening using chemicals to isolate high glutathione-producing yeast mutants. Biosci Biotechnol Biochem **76:**1085–1090. http://dx.doi.org/10.1271/bbb.110883.

59. **Nicola AM, Robertson EJ, Albuquerque P, Derengowski Lda S, Casadevall A.** 2011. Nonlytic exocytosis of *Cryptococcus neoformans* from macrophages occurs *in vivo* and is influenced by phagosomal pH. mBio **2:**e00167–11. http://dx.doi.org/10.1128/mBio.00167-11.

60. **Fortuniak A, Zadzinski R, Bilinski T, Bartosz G.** 1996. Glutathione

depletion in the yeast *Saccharomyces cerevisiae*. Biochem Mol Biol Int **38:**901–910.

61. **Zadziński R, Fortuniak A, Biliński T, Grey M, Bartosz G.** 1998. Menadione toxicity in *Saccharomyces cerevisiae* cells: activation by conjugation with glutathione. Biochem Mol Biol Int **44:**747–759. http://dx.doi.org/10.1080/15216549800201792.

62. **Valcourt JR, Lemons JM, Haley EM, Kojima M, Demuren OO, Coller HA.** 2012. Staying alive: metabolic adaptations to quiescence. Cell Cycle **11:**1680–1696. http://dx.doi.org/10.4161/cc.19879.

63. **Zaragoza O, Nielsen K.** 2013. Titan cells in *Cryptococcus neoformans*: cells with a giant impact. Curr Opin Microbiol **16:**409–413. http://dx.doi.org/10.1016/j.mib.2013.03.006.

64. **Panepinto J, Liu L, Ramos J, Zhu X, Valyi-Nagy T, Eksi S, Fu J, Jaffe HA, Wickes B, Williamson PR.** 2005. The DEAD-box RNA helicase Vad1 regulates multiple virulence-associated genes in *Cryptococcus neoformans*. J Clin Invest **115:**632–641. http://dx.doi.org/10.1172/JCI23048.

65. **Fan W, Kraus PR, Boily M-J, Heitman J.** 2005. *Cryptococcus neoformans* gene expression during murine macrophage infection. Eukaryot Cell **4:**1420–1433. http://dx.doi.org/10.1128/EC.4.8.1420-1433.2005.

66. **Hu G, Hacham M, Waterman SR, Panepinto J, Shin S, Liu X, Gibbons J, Valyi-Nagy T, Obara K, Jaffe HA, Ohsumi Y, Williamson PR.** 2008. PI3K signaling of autophagy is required for starvation tolerance and virulence of *Cryptococcus neoformans*. J Clin Invest **118:**1186–1197. http://dx.doi.org/10.1172/JCI32053.

67. **Toffaletti DL, del Poeta M, Rude TH, Dietrich F, Perfect JR.** 2003. Regulation of cytochrome *c* oxidase subunit 1 (COX1) expression in *Cryptococcus neoformans* by temperature and host environment. Microbiology **149:**1041–1049. http://dx.doi.org/10.1099/mic.0.26021-0.

68. **Ingavale SS, Chang YC, Lee H, McClelland CM, Leong ML, Kwon-Chung KJ.** 2008. Importance of mitochondria in survival of *Cryptococcus neoformans* under low oxygen conditions and tolerance to cobaltchloride. PLoS Pathog **4:**e1000155. http://dx.doi.org/10.1371/journal.ppat.1000155.

69. **Upadhya R, Campbell LT, Donlin MJ, Aurora R, Lodge JK.** 2013. Global transcriptome profile of *Cryptococcus neoformans* during exposure to hydrogen peroxide induced oxidative stress. PLoS One **8:**e55110. http://dx.doi.org/10.1371/journal.pone.0055110.

70. **Voelz K, Johnston SA, Smith LM, Hall RA, Idnurm A, May RC.** 2014. Division of labour in response to host oxidative burst drives a fatal *Cryptococcus gattii* outbreak. Nat Commun **5:**5194. http://dx.doi.org/10.1038/ncomms6194.

71. **Perfect JR, Lang SD, Durack DT.** 1980. Chronic cryptococcal meningitis: a new experimental model in rabbits. Am J Pathol **101:**177–194.

72. **Ikeda R, Sawamura K.** 2008. Bacterial and H_2O_2 stress-induced apoptosis-like events in *Cryptococcus neoformans*. Res Microbiol **159:**628–634. http://dx.doi.org/10.1016/j.resmic.2008.07.006.

73. **Dromer F, Salamero J, Contrepois A, Carbon C, Yeni P.** 1987. Production, characterization, and antibody specificity of a mouse monoclonal antibody reactive with *Cryptococcus neoformans* capsular polysaccharide. Infect Immun **55:**742–748.

74. **Murphy JW, Mosley RL, Cherniak R, Reyes GH, Kozel TR, Reiss E.** 1988. Serological, electrophoretic, and biological properties of *Cryptococcus neoformans* antigens. Infect Immun **56:**424–431.

75. **Saeed AI, Sharov V, White J, Li J, Liang W, Bhagabati N, Braisted J, Klapa M, Currier T, Thiagarajan M, Sturn A, Snuffin M, Rezantsev A, Popov D, Ryltsov A, Kostukovich E, Borisovsky I, Liu Z, Vinsavich A, Trush V, Quackenbush J.** 2003. TM4: a free, open-source system for microarray data management and analysis. Biotechniques **34:**374–378. .

76. **López S, Prieto M, Dijkstra J, Dhanoa MS, France J.** 2004. Statistical evaluation of mathematical models for microbial growth. Int J Food Microbiol **96:**289–300. http://dx.doi.org/10.1016/j.ijfoodmicro.2004.03.026.

77. **Janbon G, Maeng S, Yang D-H, Ko Y-J, Jung K-W, Moyrand F, Floyd A, Heitman J, Bahn Y-S.** 2010. Characterizing the role of RNA silencing components in *Cryptococcus neoformans*. Fungal Genet Biol **47:**1070–1080. http://dx.doi.org/10.1016/j.fgb.2010.10.005.

78. **Xue C, Liu T, Chen L, Li W, Liu I, Kronstad JW, Seyfang A, Heitman J.** 2010. Role of an expanded inositol transporter repertoire in *Cryptococcus neoformans* sexual reproduction and virulence. mBio **1:**e00084-10. http://dx.doi.org/10.1128/mBio.00084-10.

79. **Pfaffl MW.** 2001. A new mathematical model for relative quantification in real-time RT-PCR. Nucleic Acids Res **29:**e45. http://dx.doi.org/10.1093/nar/29.9.e45.